Journal of Energy Storage 115 (2025) 115989

Contents lists available at ScienceDirect

Journal of Energy Storage

journal homepage: www.elsevier.com/locate/est

Research Papers

The impact of orientation and scale of kite-shaped anisotropic metal foam layers on paraffin-based latent heat thermal energy storage units

Hakim S. Sultan Aljibori [a], Ahmad Hajjar [b], Zehba Raizah [c], Faisal Alresheedi [d], Ali Akremi [e], Ahmed Elhassanein [f], Mohammad Ghalambaz [g,h,*]

[a] College of Engineering, University of Warith Al-Anbiyaa, Karbala 56001, Iraq
[b] Center for Environmental Intelligence and College of Engineering and Computer Science, VinUniversity, Hanoi, Viet Nam
[c] Department of Mathematics, College of Science, King Khalid University, Abha, Saudi Arabia
[d] Department of Physics, College of Science, Qassim University, Buraidah 51452, Saudi Arabia
[e] Department of Chemistry, Faculty of Science, Northern Border University, Arar, Saudi Arabia
[f] Department of Mathematics, College of Science, University of Bisha, P.O. Box 551, Bisha 61922, Saudi Arabia
[g] Department of Mathematics, Saveetha School of Engineering, SIMATS, Chennai, India
[h] Laboratory on Convective Heat and Mass Transfer, Tomsk State University, 634050 Tomsk, Russia

ARTICLE INFO

Keywords:
Kite-shaped geometry
Copper metal foam
Phase change material
Anisotropic metal foams
Latent heat thermal energy storage (LHTES)

ABSTRACT

The impact of using kite-shaped anisotropic metal foam layer (AMFL) on melting heat transfer of a channel shape latent heat thermal energy storage (LHTES) unit was investigated to optimize heat transfer and conserve energy efficiently. The system employs water channels to transfer heat into a paraffin wax phase change material (PCM) via copper conduits, strategically capturing and storing surplus thermal energy. Housed within a closed 15 cm × 15 cm compartment with selective heating on one side and adiabatic boundaries elsewhere, the LHTES system integrates uniform metal foam alongside AMFL configurations varying from 25 % to 75 % of the unit's volume. The Darcy-Brinkman-Forchheimer model further elucidates fluid flow through porous media, to take into account the liquid PCM flow. Mathematical modeling utilizes finite element method solutions to simulate PCM phase change and fluid dynamics within the metal foam structure, governed by partial differential equations encompassing mass, momentum, and energy conservation principles. The optimal energy storage rate is achieved by placing the thick base of the kite-shaped AMFL at the bottom, near the hot wall. Covering 25 % and 75 % of the enclosure with an AMFL resulted in a 2.2 % and 5.6 % change in the melting rate, respectively.

1. Introduction

Phase change materials (PCMs) are essential components in thermal energy storage systems, facilitating effective heat retention and discharge at nearly uniform temperatures, which significantly improves the efficiency of energy utilization. However, the low thermal conductivity characteristic of PCMs poses a significant limitation on their practical use, as it leads to reduced rates of charging and discharging [1]. To address this limitation, a variety of methods for enhancing heat transfer have been examined, such as using fins [2–4], wire mesh [5], heat pipes [6], nanoadditives [7], or the integration of metal foams into the system. Metal foams have gained recognition as effective additives in PCM systems, attributed to their superior thermal conductivity and extensive surface area [8]. They promote more efficient heat transfer between the PCM and the surrounding environment, which in turn enhances the overall performance of the system [9].

Recent investigations have revealed notable advancements in thermal conductivity and heat transfer efficiency when metal foams are utilized in conjunction with PCMs [10]. By implementing this integration, the rates of charging and discharging are significantly expedited, which in turn leads to a heightened overall efficiency in thermal energy storage systems [11].

The advancement of heat transfer mechanisms in PCM-integrated latent heat thermal energy storage (LHTES) systems is critical for boosting their performance and ensuring their reliability. Traditional methods such as finned surfaces have been effective in increasing heat

* Corresponding author.
E-mail addresses: hakim.s@uowa.edu.iq (H.S.S. Aljibori), ahmad.h@vinuni.edu.vn (A. Hajjar), zaalrazh@kku.edu.sa (Z. Raizah), f.alresheedi@qu.edu.sa (F. Alresheedi), ali.akrmi@nbu.edu.sa (A. Akremi), m.ghalambaz@gmail.com (M. Ghalambaz).

https://doi.org/10.1016/j.est.2025.115989
Received 29 August 2024; Received in revised form 24 January 2025; Accepted 22 February 2025
Available online 27 February 2025

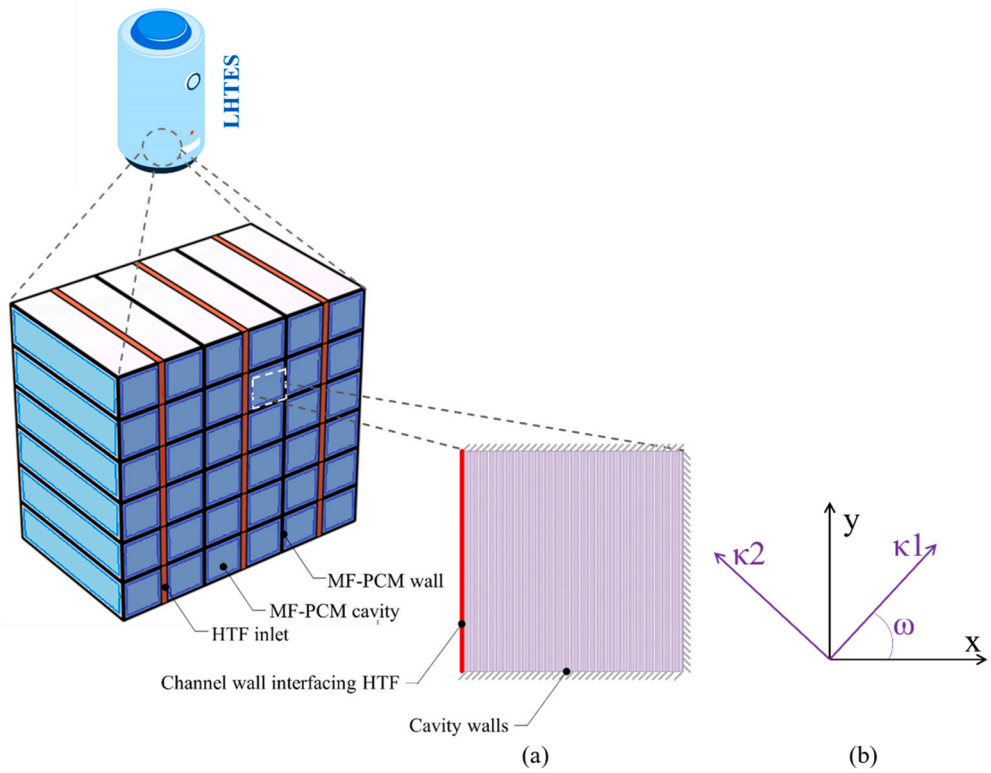

Fig. 1. Illustration of a multi-stream LHTES setup alongside a two-dimensional cross-sectional view of one individual storage compartment. (a) Visualization of the storage area layout; (b) explanation of the orientation concerning anisotropic angles (ω).

transfer area and reducing thermal resistance [12]. However, metal foams offer distinct advantages over traditional fins by providing a three-dimensional network with interconnected pores [13]. This unique structure promotes enhanced convective heat transfer and accommodates PCM impregnation, thereby maximizing heat transfer surface area and efficiency [14].

The utilization of metal foam layers in PCM-based LHTES systems has attracted considerable interest due to their unique properties and potential for tailored thermal management solutions. Metal foams, characterized by their high porosity and interconnected pore structure, offer enhanced thermal conductivity compared to solid materials [15]. This enhanced thermal conductivity is pivotal in accelerating the melting and solidification processes of PCM, crucial for efficient energy storage applications [16]. Zhao et al. [17] studied the effect of graphite foam inserts on the phase change behavior of paraffin-based thermal storage units. Authors examined various foam porosities (0.8–0.95) and configurations, revealing significant reductions in melting and solidification times for optimized designs. Thus, foam inserts can be an effective way to improve the charging and discharging time of LHTES systems with minimal foam usage.

Studies have shown that the orientation and scale of metal foam layers can profoundly impact heat transfer efficiency in PCM composites [18]. For a fixed porosity, the pore or cell size can impact the heat transfer behavior of PCM composite [19]. Anisotropic metal foams, for instance, exhibit directional preferences in heat transfer, which can be leveraged to optimize thermal energy storage systems [8]. Moreover, the scale of metal foam layers, ranging from fine to coarse pore structures, influences the overall thermal conductivity and storage capacity of PCM composites [20]. Fine-scale foams provide increased surface area for heat exchange, while coarse-scale foams offer higher storage capacity despite slightly reduced thermal conductivity [21].

The shape and configuration of metal foam layers are critical factors in optimizing heat transfer performance while minimizing weight and preserving PCM capacity. Recent advancements have explored kite-shaped anisotropic metal foam layers, which exhibit directional thermal conductivities tailored to specific applications [22]. By strategically designing the shape and orientation of metal foam layers, researchers are focused on advancing the efficiency of heat transfer and reducing the loss of capacity in PCMs typically associated with conventional heat transfer enhancement methods [23].

In recent years, significant strides have been made in enhancing the efficiency of LHTES units through the strategic integration of anisotropic metal foam layers (AMFLs). Anisotropic metal foams, characterized by their directional thermal conductivity and structural heterogeneity, offer a promising avenue for improving heat transfer rates within LHTES systems [24]. These foams are tailored with specific angles and placements within the storage units to optimize their thermal performance during both charging and discharging processes [25]. Furthermore, insights from numerical models highlight that while optimal configurations improve thermal performance, angles deviating significantly (e.g., 75°) may hinder heat transfer processes, potentially extending the phase change times [24].

The literature review demonstrates that metal foams, particularly innovative anisotropic variants, significantly enhance heat transfer rates within LHTES units. However, metal foams add weight to systems without storing latent heat, potentially reducing overall heat capacity. Anisotropic metal foams maintain a constant mass while allowing modifications in foam structure to locally enhance thermal conductivity and permeability. This engineering approach creates metal foams with tailored heat transfer characteristics in specific regions. The present study aims to address the heat transfer and energy storage behavior of a LHTES unit with a kite-shaped partial layer of anisotropic metal foam.

2. Model description

The research detailed herein displays an LHTES system, as depicted in Fig. 1, incorporating a network of channels for water circulation. Within this framework, water serves as the conduit for heat, traversing

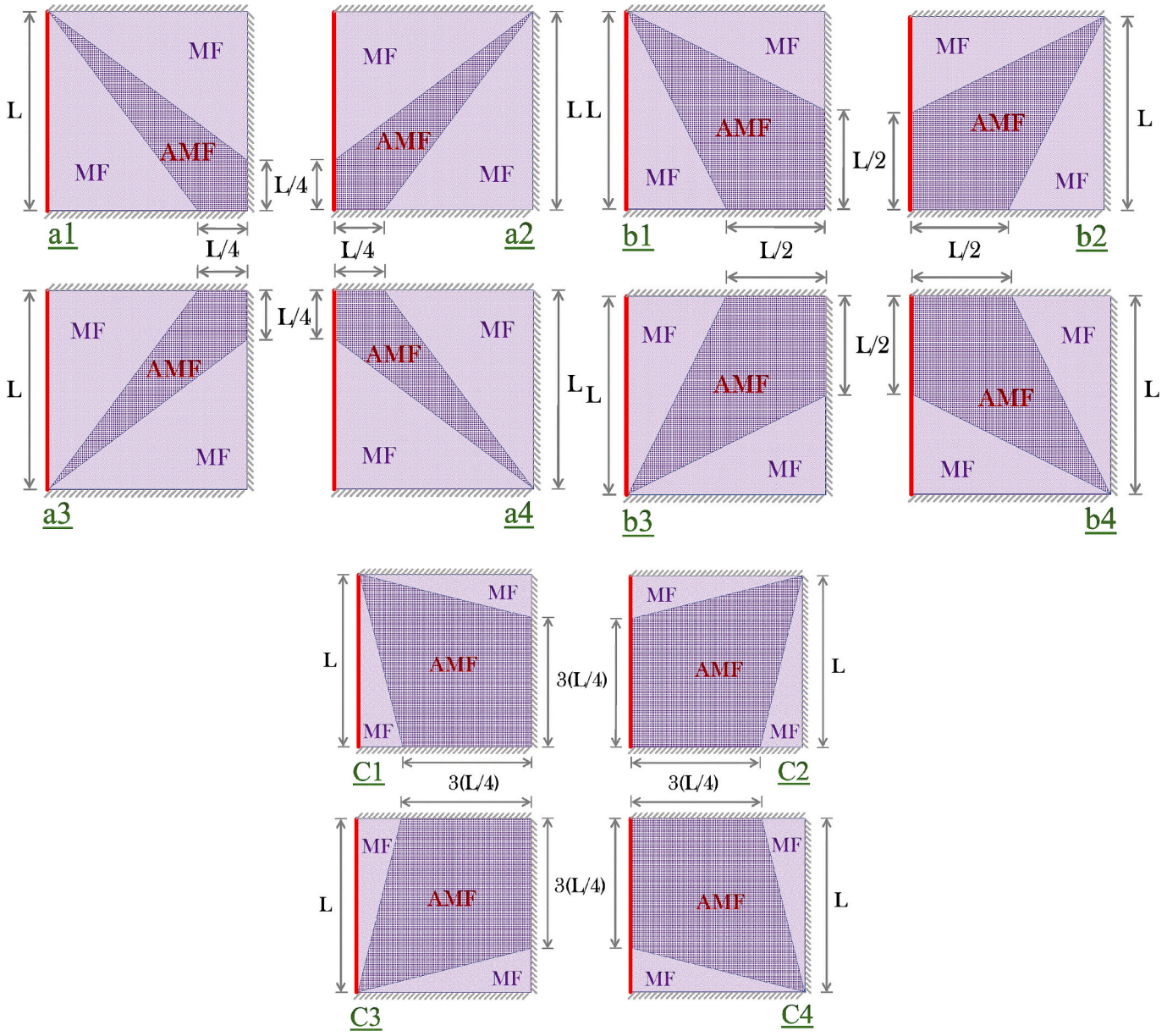

Fig. 2. Position and scale of the AMFL are shown in kite-shaped areas, occupying 25 %, 50 %, and 75 % of the total MF area in configurations (a), (b), and (c) respectively. The remaining areas display the uniform MF.

Table 1
Overview of properties for copper foam and paraffin wax.

Materials	C_p (J/kg·K)	ρ (kg/m^3)	k (W/m·K)	μ (Pa·s)	T_{fu} (K)	*Fusion enthalpy* (J/kg)
Paraffin (solid/liquid) [32–34,36]	2700/2900	916/790	0.21/0.12	0.0036	324.65	176,000
Copper foam [37]	386	8900	380	–	–	–

these pathways to transfer warmth into the paraffin wax PCM. Encased within the copper MF, the PCM assimilates heat at a higher temperature (T_h) than its fusion point (T_{fu}), transitioning from solid to liquid, and in the process, captures thermal energy with high efficiency. This configuration is designed to harvest surplus heat for future use, thereby elevating the system's capability for energy conservation and management. The system is encased in a closed 15 cm × 15 cm comportment, which applies heat to the left side while the remaining boundaries are designed to be adiabatic, preventing any heat exchange.

Fig. 2 portrays a diagrammatic view of diverse cavity designs within the LHTES, with the anisotropic metal foam (AMF) layer and the uniform metal foam, focusing on the kite-shaped AMF layer. The kite-shaped AMF layer was used because it covers a large portion of the enclosure near the boundaries, with its impact decreasing in other regions. This element is ingeniously placed to assimilate thermal energy from the heated wall and disperses it to regions distant from the heat source. The intention behind the AMFL geometry is to discover the impact of its placement and scale on the system's thermal efficiency and identify the optimal arrangement for enhancing the melting efficiency through various orientations and sizes of the AMFL in the MF structure.

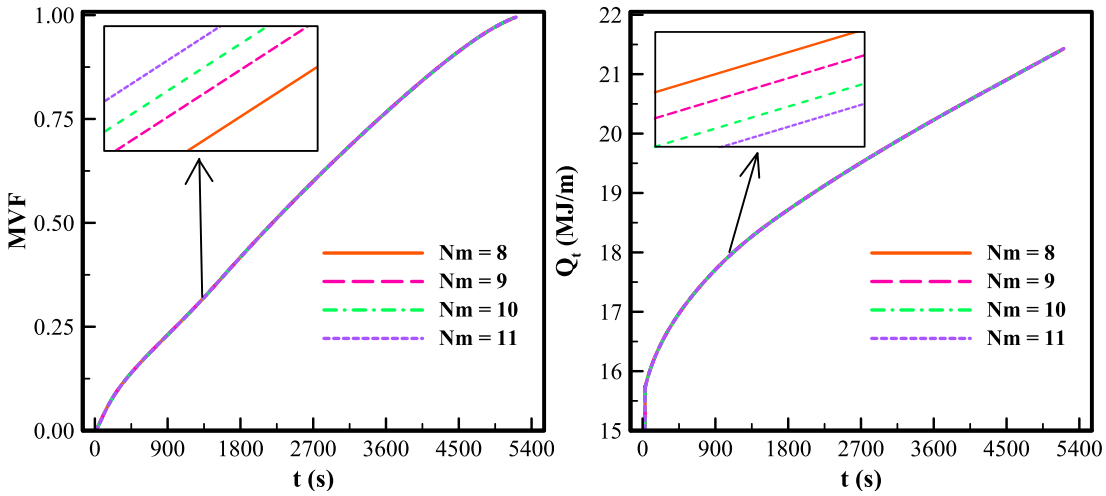

Fig. 3. Grid study: comparison of MVF and Q_t for *Nm* values of 8, 9, 10, and 11.

Table 2
Calculation durations across various scenarios of *Nm*.

Nm	Required Time
8	11 h, 22 min, and 22 s
9	14 h, 12 min, and 35 s
10	17 h, 30 min, and 52 s
11	21 h, 48 min, and 16 s

The proportion of the LHTES unit occupied by the AMFL is delineated in three distinct scenarios, 25 %, 50 %, and 75 % in configurations (a), (b), and (c), depicted in Fig. 2, demonstrating the unique kite-shaped distribution of the AMFL. Each scenario is analyzed through four different orientations, understanding the deliberate positioning of the AMFL to fine-tune melting efficiency and thermal conductivity within the PCM. The AMFL demonstrates designed directional attributes, which are determined by an anisotropy angle (ω) and an anisotropy parameter (*Kn*). The ω and *Kn* parameters for the AMFL underwent deliberate modification, with ω remaining constant at 0° and *Kn* designated at 0.3. This configuration, which denotes a perpendicular relationship to the heated wall, was utilized to investigate their effects on the thermal attributes of the various setups.

3. Governing equations

The area of study consists of three interconnected regions: the copper conduit boundary, the homogeneous MF-PCM composite, and the kite-shaped anisotropic MF-PCM composite. In terms of the liquefied PCM, it is presupposed by the model that there is an absence of slip velocity adjacent to the walls, and it functions on the premise of incompressible Newtonian fluid behavior within a two-dimensional laminar flow context. Furthermore, to tackle the correlation between density fluctuations and temperature changes in the arrangement, the model incorporates the Boussinesq approximation. During the PCM liquefaction phase, the principle of Mass Conservation is upheld by the Continuity

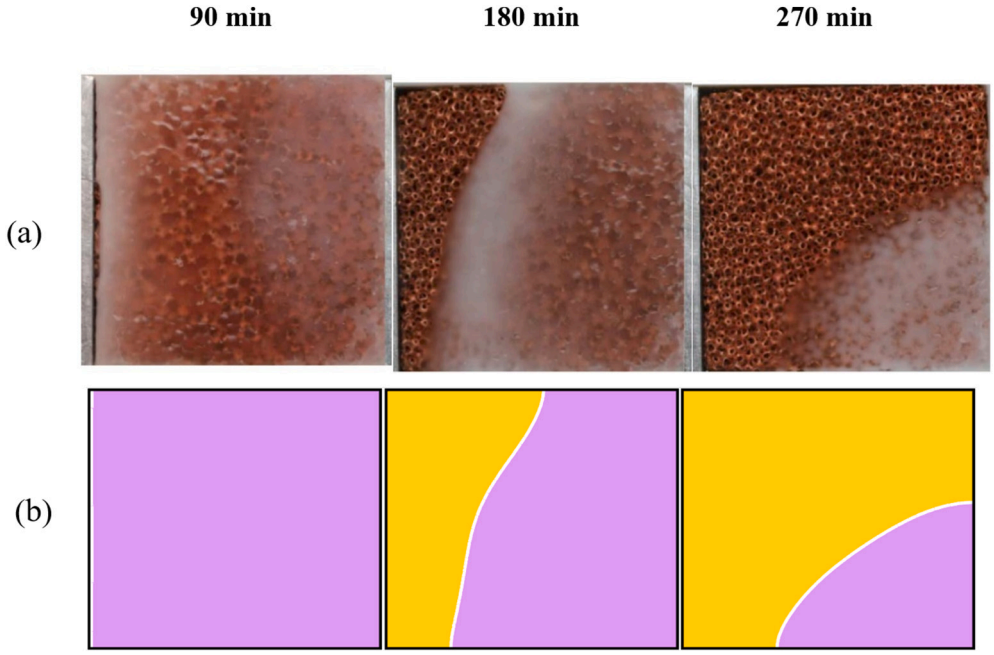

Fig. 4. Evolution of the melting process in a square cavity filled with a PCM-MF hybrid: (a) empirical data from a prior study [37], and (b) our latest research findings.

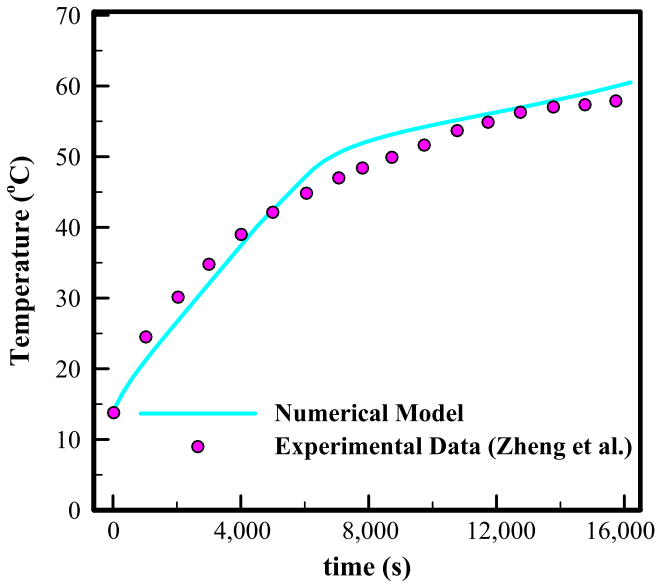

Fig. 5. Validation of this research's results through a comparative evaluation with the empirical data presented in [37].

equation, while the Momentum equation delineates the flow of liquefied PCM through the MF, taking into account both external and viscous influences. The mathematical equation of Energy elucidates on the heat absorption by the PCM during the phase change and its subsequent thermal spread within the metal foam. The Continuity, Momentum, and Energy formulas, collectively referred to as Eq. 1, as follows, adeptly simulate the PCM's melting behavior and its propagation through the MF structure [26–28]:

$$\begin{cases} \dfrac{\partial u}{\partial x}+\dfrac{\partial v}{\partial y}=0 \\ \dfrac{\partial U}{\partial t}+\dfrac{1}{\varepsilon}(U.\nabla)U=-\dfrac{\varepsilon}{\rho}\nabla P+\dfrac{\mu}{\rho}\nabla^2 U+F \\ \rho C_p\dfrac{DT}{Dt}=k\nabla^2 T+q_{gen} \end{cases} \tag{1}$$

The foundational equations governing mass, momentum, and energy conservation are represented by partial differential equations (PDEs), which are resolved by the finite element method (FEM), a technique skillfully manages the non-linear factors associated with phase transitions. The Darcy-Brinkman-Forchheimer model, which lays out a comprehensive structure for analyzing flow through porous materials, is used to depict fluid dynamics in the MF. The energy conservation function employs the local thermal non-equilibrium (LTNE) rule to independently regulate thermal diffusion between all phases of the MF and PCM. In an LTNE model, there are two temperatures fields one for MF and another one for the PCM domain. Zhao et al. [29] addressed some microscopic and averaging aspects of LTNE. To facilitate the interaction of energy across different states, source terms are incorporated to enable coupling. In areas where the PCM is in a molten state, whether in uniform or kite-shaped anisotropic configurations, natural convection phenomena are addressed through the application of continuity and momentum equations. The enthalpy-porosity technique is applied to simulate phase transformations, highlighting similarities with the semi-fluid state present in the mushy region and the dynamics of fluid flow through porous materials. In the momentum formulas, specific source terms are included by this technique to reflect the immobilization of unmelted PCM, predicted on the melt fraction (ϕ).

Consequently, the enhanced x-directional momentum equation illustrates two-dimensional flow porosity (ε) and variable density (ρ_{wax}). In response to the liquid fraction in the mushy region, this formula includes a source term to account for the impedance presented by the porous framework and the state transformation, thereby modifying fluid momentum [26–28]. The abbreviations "copper", "wax", and "eff" are respectively used to denote the metal foam made of copper, the phase change material constituted of paraffin, and their effective attributes:

$$\frac{1}{\varepsilon}\rho_{wax}\left(\frac{\partial u}{\partial t}\right)+\frac{1}{\varepsilon^2}\rho_{wax}\left(u\frac{\partial u}{\partial x}+v\frac{\partial u}{\partial y}\right)=-\left(\frac{\partial p}{\partial x}\right)+\frac{1}{\varepsilon}\mu_{wax}\left(\frac{\partial u}{\partial x^2}+\frac{\partial u}{\partial y^2}\right)$$
$$-\left(\frac{\mu_{wax}}{\kappa}\right)u-\left(\rho_{wax}\frac{C_F}{\sqrt{\kappa}}|U|\right)u+\left(A_{mush}\frac{(1-\phi(T))^2}{\gamma_{mush}+\phi^3(T)}\right)u \tag{2}$$

In the context of momentum along the y-axis, the relevant momentum equation encapsulates similar essential elements, in addition to a term for convection heat transfer, $g\rho_{wax}\beta_{wax}(T-T_0)$, highlighting the significance of buoyancy-induced flows within the molten PCM. This equation for y-directional momentum is structured as follows:

$$\frac{1}{\varepsilon}\rho_{wax}\left(\frac{\partial v}{\partial t}\right)+\frac{1}{\varepsilon^2}\rho_{wax}\left(u\frac{\partial v}{\partial x}+v\frac{\partial v}{\partial y}\right)=-\left(\frac{\partial p}{\partial y}\right)+\frac{1}{\varepsilon}\mu_{wax}\left(\frac{\partial v}{\partial x^2}+\frac{\partial v}{\partial y^2}\right)$$
$$+g\rho_{wax}\beta_{wax}(T-T_0)-\left(\frac{\mu_{wax}}{\kappa}\right)v-\left(\rho_{wax}\frac{C_F}{\sqrt{\kappa}}|U|\right)v+\left(A_{mush}\frac{(1-\phi(T))^2}{\gamma_{mush}+\phi^3(T)}\right)v \tag{3}$$

Eq. 4 is dedicated to the energy conservation in the phase change material, underscoring how heat transfer occurs convectively between the PCM and adjacent copper via $h_v(T_{copper}-T_{wax})$, and how heat is diffused through the PCM, as indicated by $k_{eff,wax}\nabla^2 T$ [30]. Additionally, the equation accounts for the latent heat of the phase transition within the PCM, represented by $\varepsilon\rho_{wax}L_{wax}\frac{\partial\phi(T)}{\partial t}$. Within these formulas [30], effective thermal conductivities for both the metal foam ($k_{\mathrm{eff,copper}}$) and phase change material ($k_{\mathrm{eff,wax}}$) are utilized, showing the role of pore structures in influencing thermal conductivity.

$$\varepsilon(\rho C_p)_{wax}\frac{\partial T_{wax}}{\partial t}+(\rho C_p)_{wax}\left(u\frac{\partial T_{wax}}{\partial x}+v\frac{\partial T_{wax}}{\partial y}\right)=$$
$$k_{eff,wax}\left(\frac{\partial^2 T}{\partial x^2}+\frac{\partial^2 T}{\partial y^2}\right)+h_v(T_{copper}-T_{wax})-\varepsilon\rho_{wax}L_{wax}\frac{\partial\phi(T)}{\partial t} \tag{4}$$

In the MF phase, the equation is crafted to illustrate the conservation of energy, where the term $(1-\varepsilon)(\rho C_p)_{copper}$ is used to articulate the copper foam's effective heat capacity, factoring in porosity (ε):

$$(1-\varepsilon)(\rho C_p)_{copper}\frac{\partial T_{copper}}{\partial t}=k_{eff,copper}\left(\frac{\partial^2 T_{copper}}{\partial x^2}+\frac{\partial^2 T_{copper}}{\partial y^2}\right)+h_v(T_{wax}-T_{copper}) \tag{5}$$

Within the specified governing equations, a variety of parameters are employed, including porous permeability (κ), the fusion latent heat (L), the Forchheimer coefficient (C_F), and the coefficient of thermal expansion (β). The thermophysical characteristic of the PCM have been computed using the linear wight average of properties solid and liquid PCM as:

$$(\rho C_p)_{wax}=\varphi(\rho C_p)_s+(1-\varphi)(\rho C_p)_l \tag{6}$$

$$\rho_{wax}=\varphi\rho_s+(1-\varphi)\rho_l \tag{7}$$

In these equations, the melted and unmelted states of the phase change material are denoted by l and s, respectively. Within the context of the melting progression, the Carman-Kozeny equation, identified through the parameter A_{mush}, plays a pivotal role in controlling the velocities of the PCM. A high value of $A_{mush}=1\times10^{10}$ Pa·s/m^2 is used to impose significant resistance to the movement of the PCM and prevent its motion in the solid regions. The high value of A_{mush} is essential because the fluid moves through a porous domain (metal foam), which already has high Darcy resistance. Therefore, the A_{mush} value must

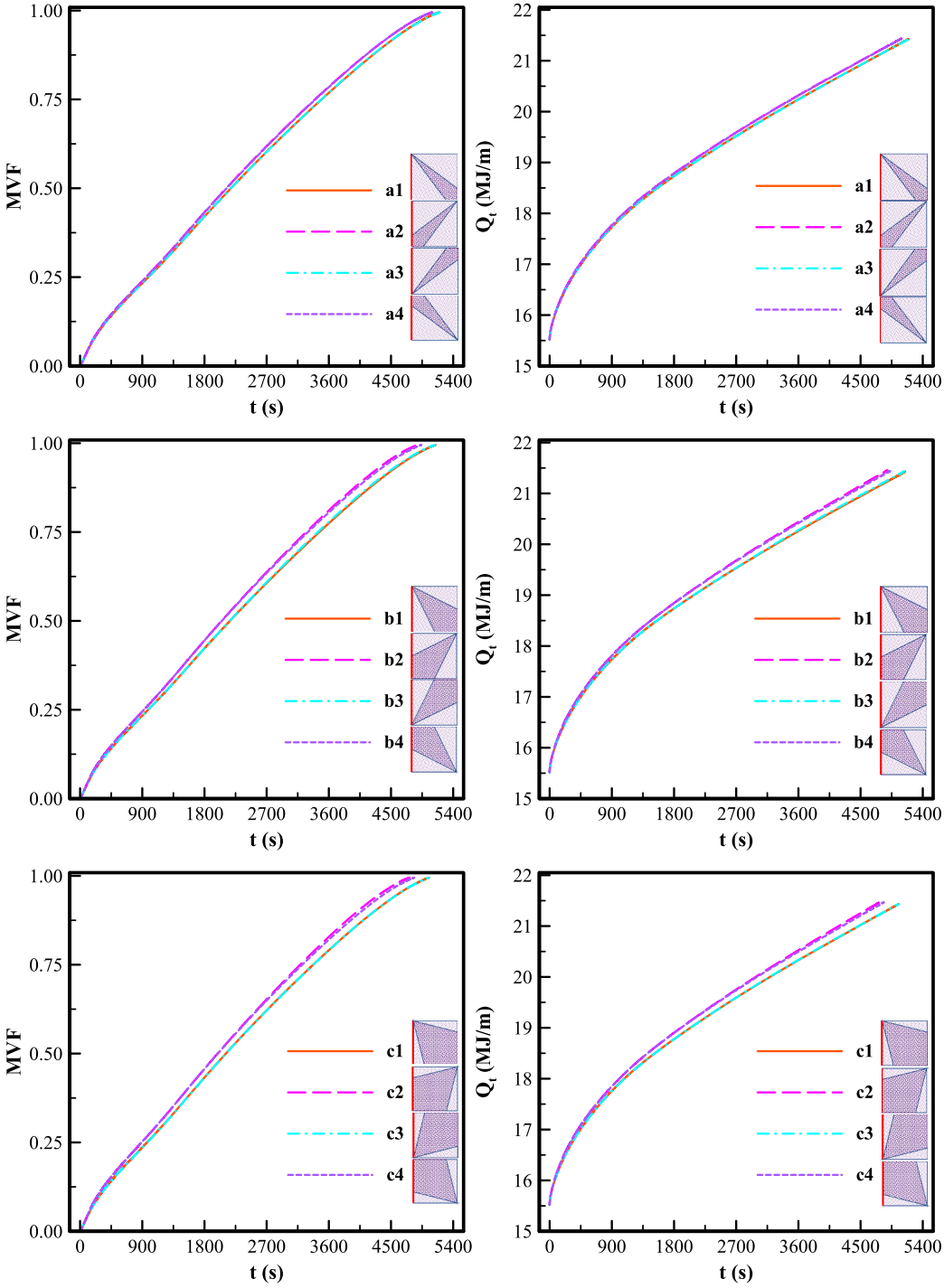

Fig. 6. MVF, total heat transfer (Q_t) over the melting progression for different configurations.

Table 3
The complete melting time for each configuration.

Cases	AMFL occupied %	80 % charging	90 % charging	99.5 % charging
a1	25 %	3782 s	4399 s	5192 s
a2	25 %	3682 s	4297 s	5093 s
a3	25 %	3777 s	4393 s	5205 s
a4	25 %	3689 s	4298 s	5089 s
b1	50 %	3744 s	4354 s	5145 s
b2	50 %	3542 s	4122 s	4890 s
b3	50 %	3722 s	4330 s	5132 s
b4	50 %	3572 s	4164 s	4938 s
c1	75 %	3652 s	4257 s	5050 s
c2	75 %	3447 s	4014 s	4767 s
c3	75 %	3654 s	4257 s	5047 s
c4	75 %	3486 s	4072 s	4836 s

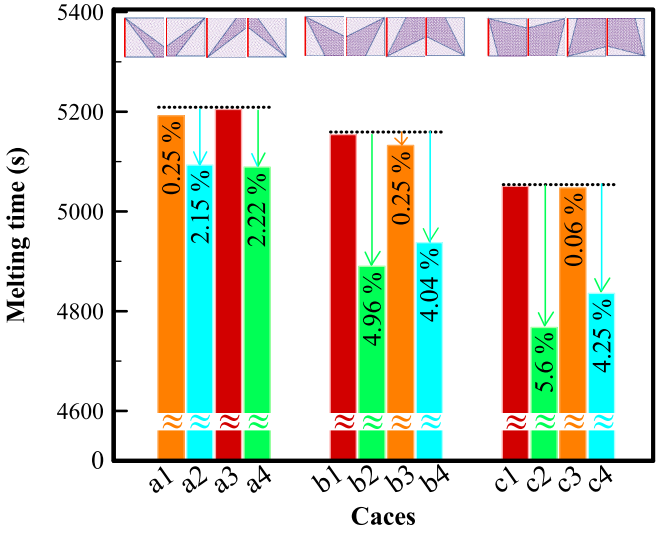

Fig. 7. The total melting times across different configurations. Each column's percentage indicates the decrease in melting time relative to the least efficient configuration at corresponding scales, highlighted in red, with the most efficient designs marked in green. (For interpretation of the references to color in this figure legend, the reader is referred to the web version of this article.)

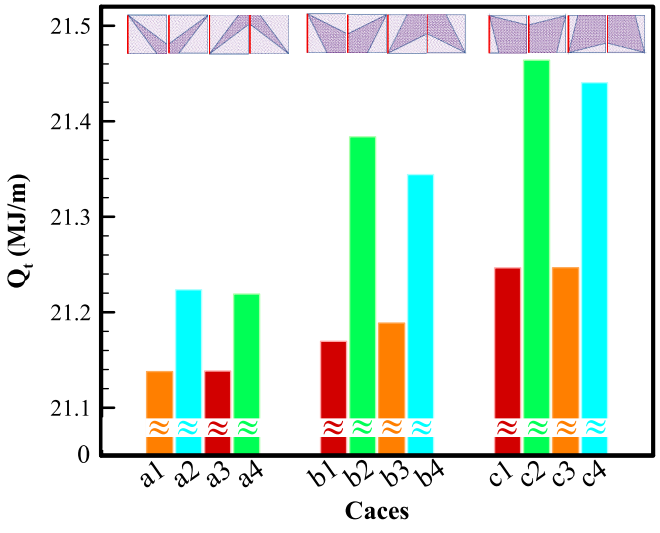

Fig. 8. The total energy stored at t = 80 min for different configurations. Columns in red in each scale represent the least efficient designs, while those in green indicate the most efficient. (For interpretation of the references to color in this figure legend, the reader is referred to the web version of this article.)

impose even larger resistive forces than those in the porous media. The model treats the mushy zone as a porous framework, where altering from melted to unmelted areas significantly diminishes the porosity and permeability, leading to a near-zero fluid velocity. This illustrates the body force's damping effect within this region. Additionally, a lesser constant, γ_{mush}, set at 0.001, is incorporated to avoid scenarios involving division by zero, playing a critical role in the model's functionality. The melting volume fraction, ϕ, dependent on temperature, outlines this relationship as follows [2]:

$$\phi(T)=\begin{cases}0 & T<T_{fu}-\dfrac{\Delta T_{fu}}{2} \quad \text{(Solid wax)}\\ \dfrac{1}{2}+\dfrac{(T-T_{fu})}{\Delta T_{fu}} & T_{fu}-\dfrac{\Delta T_{fu}}{2}\le T\le T_{fu}+\dfrac{\Delta T_{fu}}{2} \quad \text{(Mushy zone)}\\ 1 & T>T_{fu}+\dfrac{\Delta T_{fu}}{2} \quad \text{(Liquid wax)}\end{cases} \tag{8}$$

In the mushy zone, the function $\phi(T)$ takes a linear form, where T_{fu} is the fusion temperature and ΔT_{fu} is the temperature range over which the PCM transitions from solid to liquid. In this zone, the PCM is neither fully solid nor fully liquid, where both phases coexist. Velocity within this framework is redefined as $\mu = (1-\phi)\times a + \mu_{wax,l}\,\phi$, where a is assigned a substantially high value (10^4 Pa·s), making viscosity approach the liquid PCM's standard dynamic viscosity, $\mu_{wax,l}$, when ϕ is equal to 1. In contrast, as ϕ drops to 0, the viscosity markedly rises in the unmelted regions, thereby bolstering flow resistance [2]. The equation cited in various sources [26,30] was utilized to ascertain the effective thermal conductivity of the PCM. The given range for the porosity suggests that the MF is quite porous.

$$k_{eff,\ wax}=\frac{1}{3}k_{wax}(2+\varepsilon)\quad 0.929<\varepsilon<0.974 \tag{9}$$

Although PCM and metal foam are distinct phases with different temperature fields, the presence of one phase (in this case, MF) affects the thermal conductivity of the other phase, PCM. Therefore, following the literature studies, the effective thermal conductivity should be considered for each phase separately.

In the design of the kite-shaped AMFL, the model acknowledges changes in thermal conductivity and permeability in different orientations. Such variations are driven by the anisotropy angle (ω) and the anisotropic parameter (Kn), since the ligaments within the metal foam later are intentionally strengthened along a specific direction, enhancing thermal conductivity while reducing permeability. These equations below describe the anisotropic behavior, with trigonometric functions of the ω used to translate the properties between the principal and the actual directions. This is done by creating a second-order tensor that relates the intrinsic properties k_1 and k_2 with the anisotropy angle inside the system, as elaborated in the subsequent equations [31]. In the context of copper MF, the signs κ_m and k_m denote the average permeability and thermal conductivity and, respectively, as derived from the methodologies outlined in references [32–34]:

$$\kappa=\begin{bmatrix}\kappa_2(sin\omega)^2+\kappa_1(cos\omega)^2 & (\kappa_1-\kappa_2)(cos\omega)(sin\omega)\\ (\kappa_1-\kappa_2)(cos\omega)(sin\omega) & \kappa_2(cos\omega)^2+\kappa_1(sin\omega)^2\end{bmatrix} \tag{10}$$

$$k_{eff,copper}=\begin{bmatrix}k_2(sin\omega)^2+k_1(cos\omega)^2 & (k_1-k_2)(sin\omega)(cos\omega)\\ (k_1-k_2)(sin\omega)(cos\omega) & k_2(cos\omega)^2+k_1(sin\omega)^2\end{bmatrix} \tag{11}$$

The anisotropy factor is represented by Kn, where a value of Kn = 0 signifies an isotropic MF. $\kappa_1 = (1-Kn)\times\kappa_m$, $\kappa_2 = (1+Kn)\times\kappa_m$ are the equations for permeability, while $k_1 = (1+Kn)\times k_m$ and $k_2 = (1-Kn)\times k_m$ represent the metal foam's thermal conductivity and permeability, respectively. To maintain the MF's structural integrity, it is critical to regulate the anisotropic factor at a practical level. In this study, Kn = 0.3, $\omega = 0°$, $\varepsilon = 0.95$, and pore per inch of 5 were selected for analysis of the results. The average effective thermal conductivity (k_a) and

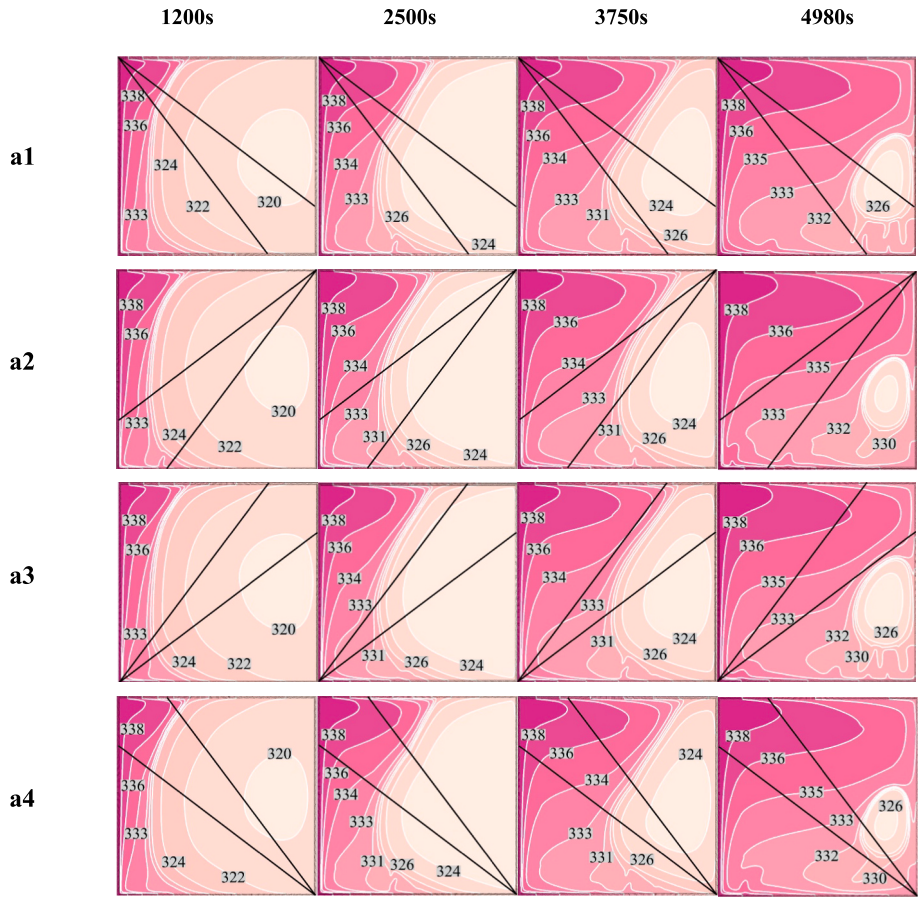

Fig. 9. Isotherms (K) and MVF contours for configurations (a), where the kite-shaped AMFL occupies 25 % of the total MF. The yellow area shows the molten PCM, while the purple area signifies the solid PCM in the MVF contour. (For interpretation of the references to color in this figure legend, the reader is referred to the web version of this article.)

permeability (κ_a) of the metal foam were thus calculated, incorporating insights from prior research [26,30,35]:

$$\kappa_a = \frac{1}{(\kappa_{tor}-1)\kappa_{tor}}\left(\frac{\varepsilon d_{fp}\sqrt{\frac{\kappa_{tor}}{3\varepsilon}}}{6}\right)^2 \tag{12}$$

$$k_a = \frac{1}{3}k_{copper}(1-\varepsilon) \tag{13}$$

The inclusion of additional equations that include κ_{tor} and d_{fs} is essential. These equations are significant in evaluating the thermal conductivity of copper (k_{copper}), the characteristic parameter (d_{fp}) for pore density (pores per inch), and the comprehensive thermal conductivity of the metal foam (Table 1), as cited in [35].

$$\frac{1}{\kappa_{tor}} = \frac{(9-8\varepsilon)^{\frac{1}{2}}}{2\varepsilon}cos\left\{\frac{4\pi}{3}+\frac{1}{3}cos^{-1}\left(\frac{8\varepsilon^2-36\varepsilon+27}{(9-8\varepsilon)^{\frac{3}{2}}}\right)\right\}d_{fp}+\frac{3}{4\varepsilon} \tag{14}$$

$$\frac{d_{fs}}{d_{fp}} = \left(\frac{59}{50}\right)\left(\frac{1}{1-exp(25(\varepsilon-1))}\right)\left(\frac{1-\varepsilon}{3\pi}\right)^{\frac{1}{2}} \tag{15}$$

$$d_{fp} = \frac{0.0254}{\mathrm{PPI}} \tag{16}$$

The assessment included the calculation of the Forchheimer coefficient (C_F) as described below [35]:

$$C_F = \left(\frac{d_{fs}}{d_{fp}}\right)^{-1.63}(1-\varepsilon)^{-0.132}\times 0.00212 \tag{17}$$

The melted volume fraction (MVF) is used to track the progress of melting in a PCM, an important aspect in LHTES systems, where the PCM absorbs and releases thermal energy storage during phase changes. Expressed as a dimensionless quantity, the MVF quantifies the extent to which the PCM has undergone liquefaction, relative to its total volume. The calculation of the MVF is derived from the integral ratio over the prescribed volumetric domain. A value of zero indicates that the PCM remains entirely solid, whereas a value of one signifies that the PCM has fully transitioned to a liquid state.

$$\mathrm{MVF} = \frac{\oint_V(\varepsilon\varphi)dV}{\oint_V(\varepsilon)dV} \tag{18}$$

The power of energy storage defines the rate at which energy is stored in the system, which can be calculated as the total stored energy (Q_t) divided by the time over which the energy is stored. The aggregate energy retained, referred to as Q_t, is identified as the collective sum of sensible (Q_{sensible}) and latent (Q_{latent}) heat energies.

$$\mathrm{Power} = Q_t/time \tag{19}$$

$$Q_t = Q_{\mathrm{sensible}} + Q_{\mathrm{latent}} \tag{20}$$

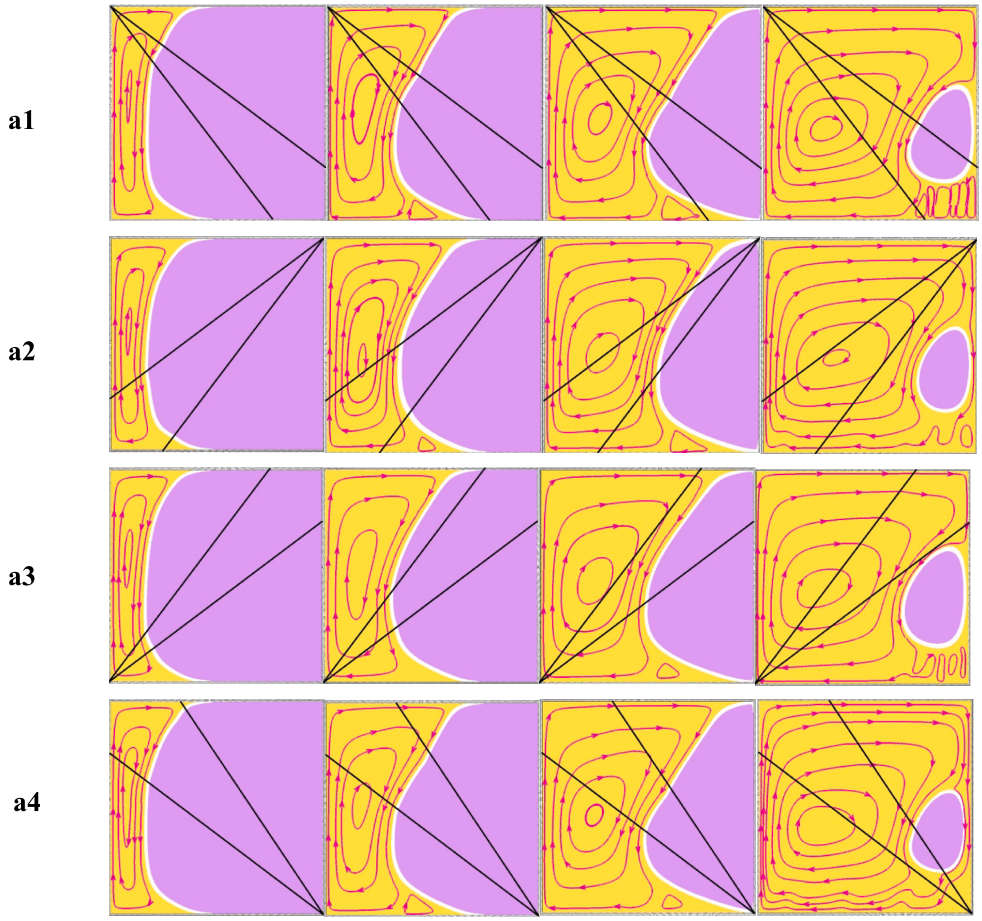

Fig. 9. (*continued*).

$$Q_{\text{sensible}} = (T - T_0)(\rho C_P)_{\text{copper}} \oint_V (1-\varepsilon)dV + \oint_V \left(\int_{T_0}^{T} \varepsilon(\rho C_P)_{wax}(T)dT \right) dV + (T - T_0)(\rho C_P)_{\text{Wall}} V_{\text{Wall}} + (T - T_0)(\rho C_P)_{\text{HTF}} V_{\text{HTF}} \tag{21}$$

$$Q_{latent} = \varepsilon \oint_V (\rho_{wax} \varphi L_{wax}) dV \tag{22}$$

The integral terms presented in Eq. 21 account for the energy stored due to the temperature difference between the current and initial states, factoring in both the solid and liquid fractions of the PCM as well as the heat transfer fluid and the system's wall, while the integral shown in Eq. 22 calculates the total latent heat stored in the PCM as it changes phase from solid to liquid or vice versa.

4. Grid study

To assess the influence of grid density on computational precision, the researchers explored the melting of PCM using configurations (a1) with parameters $Kn = 0.3$ and $\omega = 0°$. Given the increasing computational demands associated with higher mesh resolutions, particularly due to the growth in quadrilateral and edge elements, a mesh setting of $Nm = 10$ was selected for the subsequent calculations. This setting is preferred as it provides an effective compromise between precision and computational time, totaling 17 h and 30 min. The computational domain was segmented using an unstructured grid, where the parameter Nm governs the grid density. Fig. 3 exhibits the MVF and overall thermal transmission for grid scales ranging from $Nm = 8$ to $Nm = 11$ throughout the melting phase. As the grid becomes denser, indicated by increasing Nm values, the computational burden also heightens. For instance, at $Nm = 11$, the duration required for melting calculations extends to 21 h and 48 min, compared to a reduced time of 11 h and 22 min at $Nm = 8$. The table in Fig. 2 details each grid configuration and the corresponding times needed to achieve complete melting (Table 2).

5. Model verification

In their investigative study, Zheng et al. [37] analyzed a system comprised of copper MF and paraffin PCM, housed within a 10 × 10 × 3 cm enclosure. This system, characterized by its isotropic MF structure, was examined to assess thermal responses under three distinct thermal conditions, focusing on heat delivery to the PCM composite's top, bottom, and left interfaces. The scenario considered for validation involves the composite's left boundary, which is exposed to a controlled thermal flux of 1150 W at a heating rate of 10 °C/min, while the remaining walls are thermally insulated. Operating under a laminar flow regime within a temperature range of 20 to 80 °C, the system exhibited significant thermal activity, characterized by a matrix density of 5 pores/in. and a porosity level of 0.95 in the metal foam. Fig. 4 captures the phase change dynamics from liquid to solid at various times throughout the melting progression. The simulation results, including the structural nuances, edge definitions, and thermal gradients, exhibit a noteworthy alignment with the research outcomes documented by Zheng et al. in reference [37]. Fig. 5 also depicts a comparison of the mean temperature profile, measured along the vertical line 2.5 cm from the heat application plane, with experimental data plotted against the numerical simulation over time.

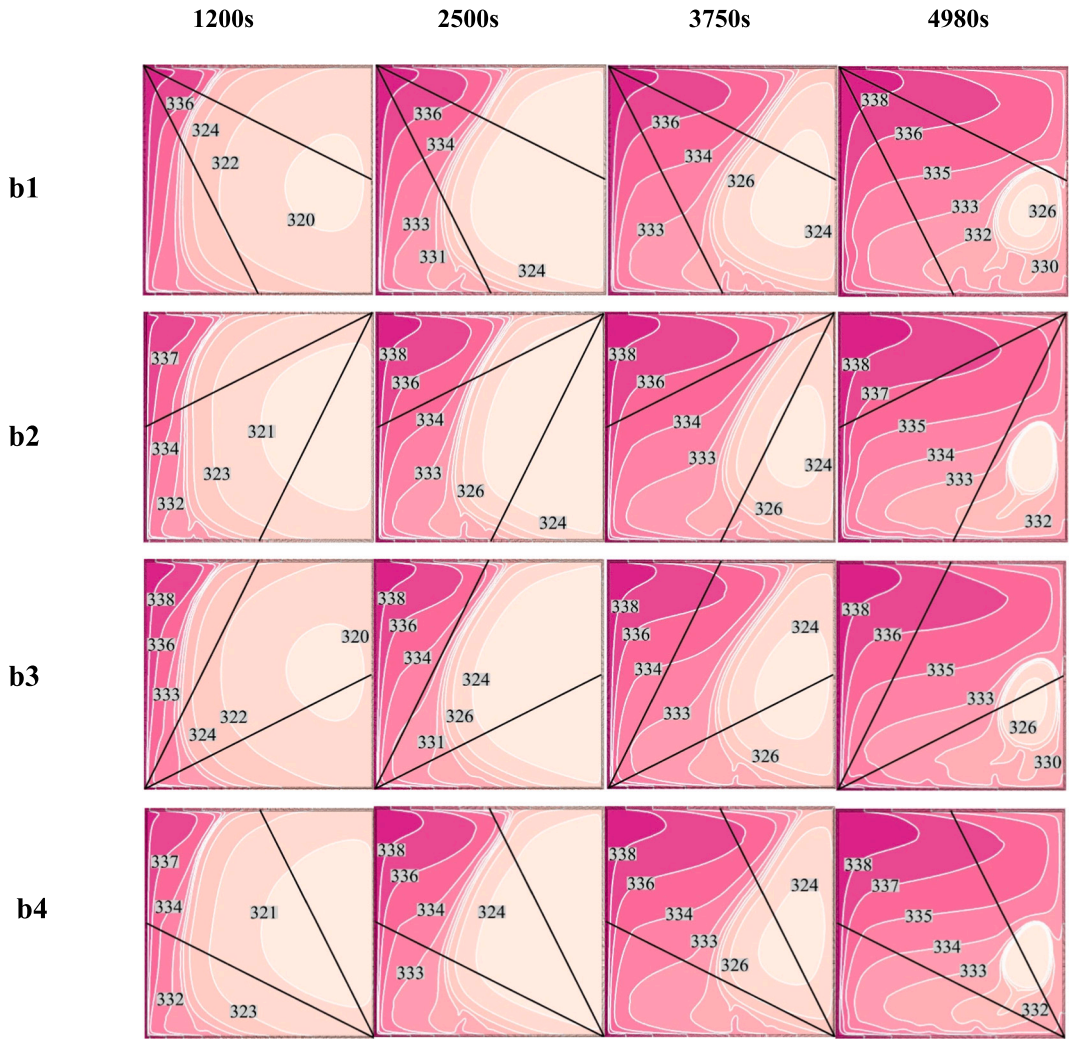

Fig. 10. Isotherms (K) and MVF contours for configurations (b), where the kite-shaped AMFL occupies 50 % of the overall MF. The yellow zone represents the molten PCM, and the purple zone indicates the solid PCM in the MVF contour. (For interpretation of the references to color in this figure legend, the reader is referred to the web version of this article.)

6. Results and discussion

Initially, the study quantifies and discusses the effects of AMFL size and orientation on the melting fraction, melting duration, and energy storage capacity. This is followed by a graphical depiction of the variations in flow and thermal patterns within the cavity across different AMFL configurations, to elucidate their impact on the observed phenomena of melting and energy storage.

Fig. 6 depicts the variations of the MVF and the total energy stored Q_t as functions of time for the different configurations of the AMFL. The MVF initially starts at 0 where all the PCM is in the solid state, then it increases gradually as the PCM melts until finally reaching 1 when all the material is in the liquid phase. A slight difference between the MVF curves for different AMFL orientations is observed in the case (a), where the AMFL occupies 25 % of the total MF volume. The impact of changing the orientation becomes more apparent when the AMFL percentage is increased to 50 %, case (b) and to a higher extent at 75 %, case (c). This first observation indicates that the presence of anisotropy in the porous foam can indeed alter the PCM melting. More quantitative comparison between the different orientations of the AMFL layer will be provided in subsequent figures. As for Q_t, it follows the variation of the MVF, as the more PCM melts, the more it absorbs energy in the form of latent heat and consequently heat transfer rises. Initially, Q_t increases sharply, then the slope of its variation becomes less sharp, when the remaining volume of solid PCM undergoes melting shrinks. It is noted in cases a, b, and c that, the configurations 2 and 4 lead to higher MVF and Q_t than the configurations 1 and 3. In 2 and 4, the kite-shaped AMFL is oriented in a way that its larger side is close to the hot wall, while the opposite is found in 1 and 3. Therefore, the presence of anisotropy in the area neighboring the hot wall seems to improve melting and heat transfer, which is related to the changes in permeability orientation. Having (a) large part of the AMFL near the hot wall has more impact in this regard as PCM starts to melt in that region, where the resulting convective flow is initiated. Due to anisotropy, the permeability along the flow direction is enhanced, leading to a higher convective flow intensity.

A summary of melting duration for different melting percentages is presented in Table 3 for the various configurations of the AMFL. Among all the considered configurations, the shorted melting time is obtained in c2, while the longest one is in a3. In the former, the AMFL occupies 75 % of the cavity and its largest side is near the hot wall, while in the latter it occupies 25 % of the total volume and its smaller side is at the heated wall. Moreover, it is seen that for every AMFL orientation (1 to 4), the melting time is reduced when the percentage of AMFL is raised (a to c). Additionally, for every AMFL percentage (a, b and c), the melting duration is increased when the large side of the AMFL is placed at the right of the cavity (1 and 3 compared to 2 and 4). These outcomes

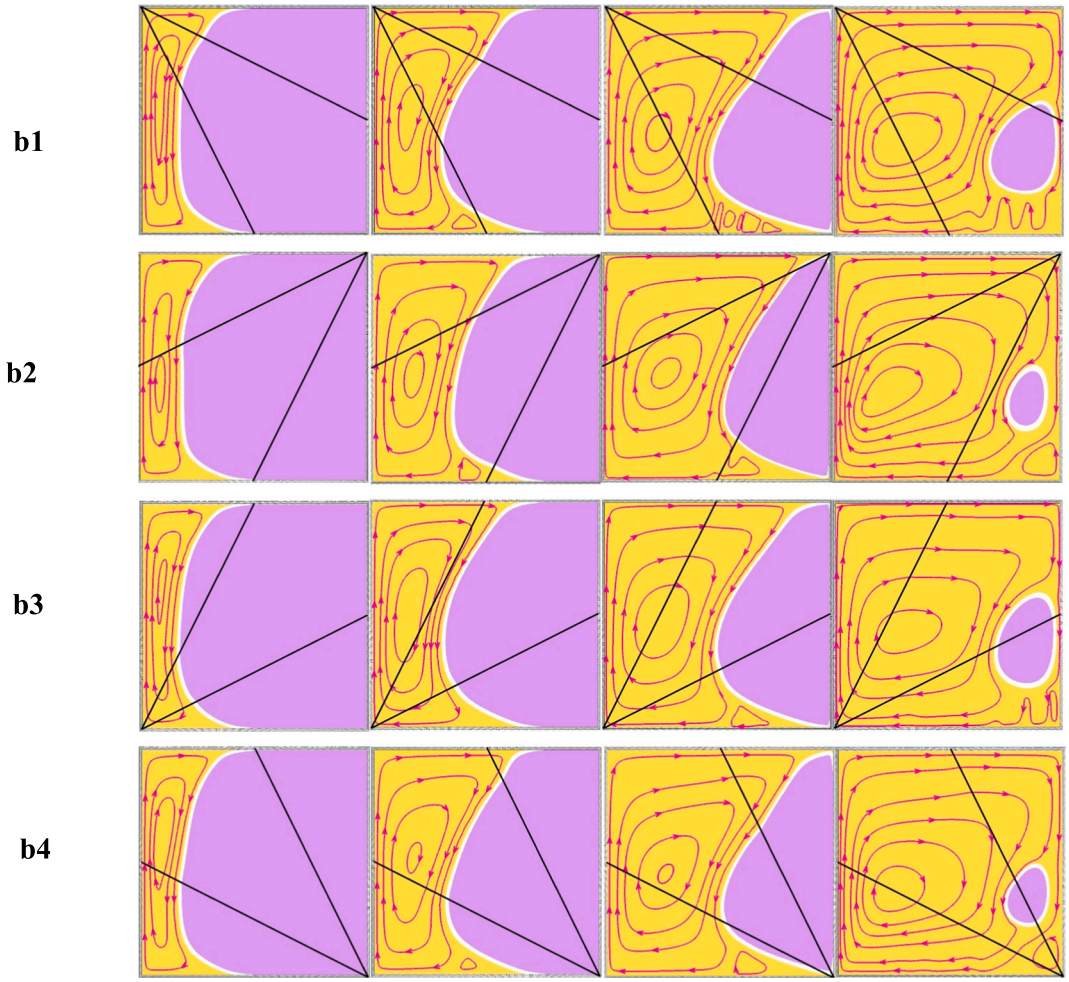

Fig. 10. (*continued*).

confirm the observations discussed in Fig. 6.

To provide a quantitative comparison, the percentage of reduction in melting time relative to the least efficient configuration for each AMFL size is illustrated in Fig. 7. In case (a), the difference between the least (a3) and most (a4) efficient configurations is 2.22 %, indicating that when the AMFL size is small, the impact of its orientation is limited. At an AMFL percentage of 50 %, utilizing a kit-shaped AMFL with the larger side placed in the bottom left corner results in a 4.96 % reduction in melting duration compared to the configuration where the larger side is at the bottom right. Similarly, in case 6, placing the large side of the AMFL at the bottom left (c2) increases the melting speed by 5.6 % compared to the case c1. These results show that altering the permeability orientation near the hot wall can indeed improve the PCM melting.

From an energy point of view, Fig. 8 shows the total energy stored Q_t after 80 min in each configuration with indications to the most and least efficient designs. For each case, the lowest Q_t is found in orientations 1 and 3, where the large side of the kite-shaped layer is on the right side of the enclosure. In addition, for each case (a, b and c), the highest Q_t is obtained in cases 2 and 4.

It is also worth noting that Q_t can still be increased even if the AMFL size was reduced. For instance, Q_t in case b2, where the AMFL percentage is 50 %, is higher than its value in cases c1 and c3, where the AMFL percentage is 75 %. The difference is that in b2, the large side of the AMFL is at the hot wall, while the opposite is observed in c1 and c3. This observation indicates that the orientation of the AMFL is as important as its size and that raising the size alone is not enough to lead to the optimal melting and energy storage.

Fig. 9 illustrates the isothermal and MVF contours at different instants in the configuration (a) where the AMFL occupies 25 % of the total MF. Initially, the PCM starts to melt along the left hot wall as the temperature is higher than the PCM's fusion temperature, where the isotherms are vertical indicating that heat transfer is dominated by conduction. As time goes, melting intensifies and its interface moves toward the right, and a shift in the shape of the isotherms around the center of the cavity, pointing out a dominance of convective heat transfer. This is also shown by the flow streamlines depicting a clockwise recirculation zone in the melted PCM, resulting from the hotter PCM ascending and getting replaced by colder one moving downwards. Finally, after 5000 s, most of the PCM in the cavity has melted and undergoing convective flow and heat transfer, except a small portion near the cold wall which remains in the solid phase. It can be seen that the size of the non-melted PCM portion is smaller in the cases a2 and a4 compared to the cases a1 and a3, which confirm the fact that placing the kite-shaped anisotropic porous layer with its larger side near the hot wall leads to more melting in the cavity, due to the improvement in the convective flow circulation which mainly starts and occurs in the region neighboring the heated boundary.

The isotherms and MVF contours are depicted in Figs. 10 and 11 for the configurations where the AMFL occupies 50 % and 75 % of the total MF, respectively. In these cases, similar observations to the ones discussed in Fig. 9 are noted, regarding the shape and distribution of the isotherms, as well as the melting behavior. Nonetheless, it is seen that the size of the remaining solid PCM after melting is the smallest in

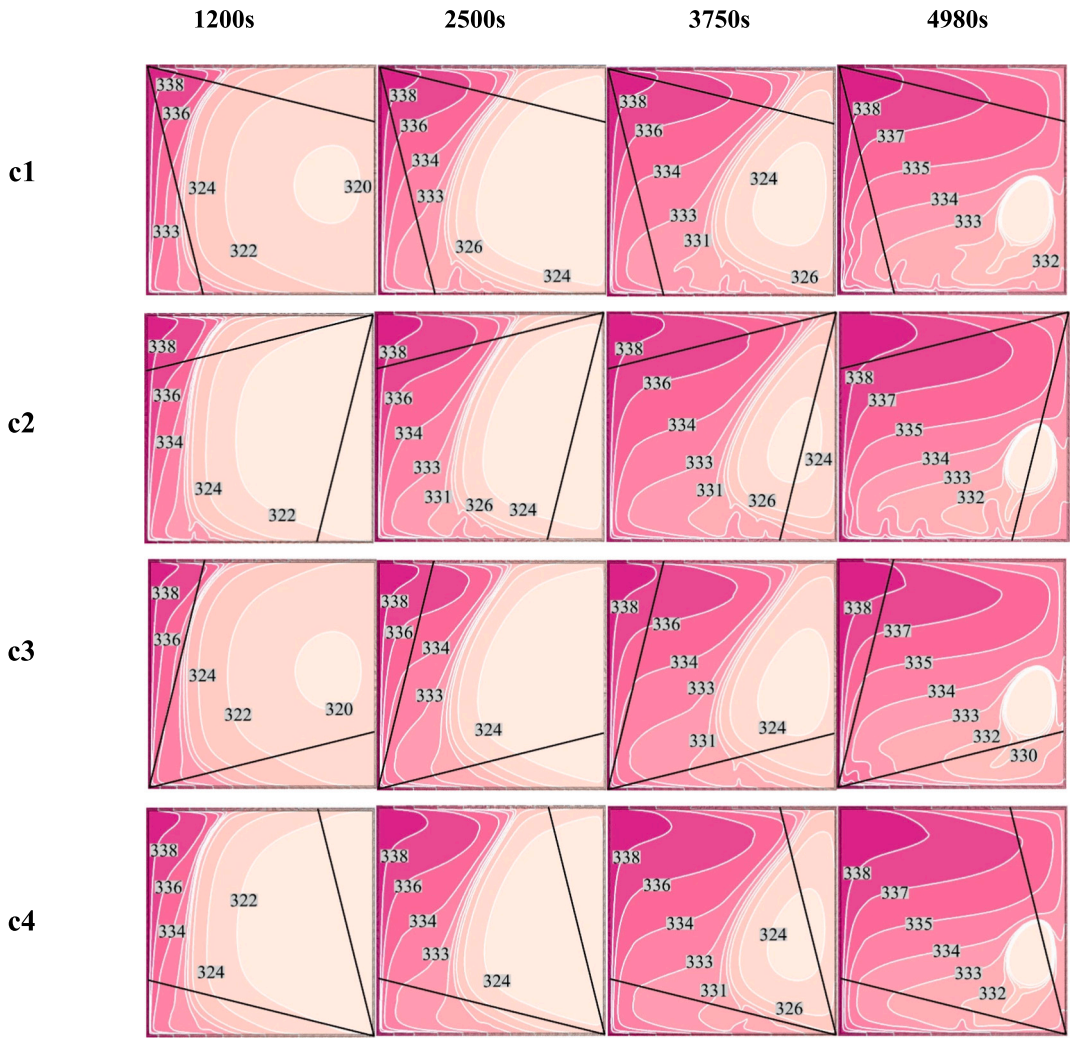

Fig. 11. Isotherms (K) and MVF contours for configurations (b), where the kite-shaped AMFL fills 75 % of the total MF. In the MVF contour, the yellow section illustrates the molten PCM, whereas the purple section denotes the solid PCM. (For interpretation of the references to color in this figure legend, the reader is referred to the web version of this article.)

Fig. 11, compared to the other figures, for all the orientations of the AMFL. This also confirms the contribution of the AMFL to the improvement of PCM melting and strengthens the conclusion that the optimal configuration among the tested ones is a kite-shaped AMFL that covers 75 % of the cavity and which has its larger side oriented toward the hot wall.

In all the figures from 9 to 11, comparing the configurations 2 to 3, for instance, reveals that the former presents more disturbance in the isotherms near the bottom left edge in the initial stages of melting where the convective flow initiates, which indicates the impact of the AMFL layer on the PCM behavior. In fact, in configuration 2, the larger side of the layer is at the left side of the enclosure, which improves the initial fluid circulation in that zone compared to the MF layer, which confirms the ability of changing the porous material structure to affect the flow and heat transfer in the PCM.

7. Discussion and conclusions

The present study addressed a technique to improve the efficiency of LTHES systems, by adding a kite-shaped anisotropic metal foam layer. Specifically, a square PCM-filled cavity heated from its left wall and insulated on its other walls, containing a metallic foam, was analyzed. In this MF, different configurations of the kite-shaped AMFL were considered. These configurations correspond to various sizes of the AMFL, where it can cover 25 %, 50 %, or 75 % of the total MF size, as well as to different orientations of the kite-shape, where its large side can be placed at one of the four corners of the enclosure. The equations governing the flow and heat in the cavity were derived and solved using the finite element method. The results indicate that including an AMFL in the cavity can indeed alter the PCM melting behavior and the corresponding energy stored. This outcome is particularly important because the AMFL does not change the porosity of the medium, but only the direction of permeability. In other words, melting and energy storage can be changed without having to change the amount of metal used and the storage capacity. Rather, changing the structure of the foam can be effective. It was obtained that by increasing the size of the AMFL, the PCM melting can be accelerated, and the energy storage can be enhanced. Nonetheless, it was also found that the size alone of the AMFL is not the only important parameter, but also its orientation. In particular, the fastest melting and the highest energy stored can be observed in the case where the AMFL is placed with its larger side at the bottom left, near the hot wall. When this layer occupied only 25 % of the cavity space, only 2.2 % difference was found between the least and most efficient configurations. This percentage raised to 5.6 % when the AMFL layer covers 75 % of the cavity space.

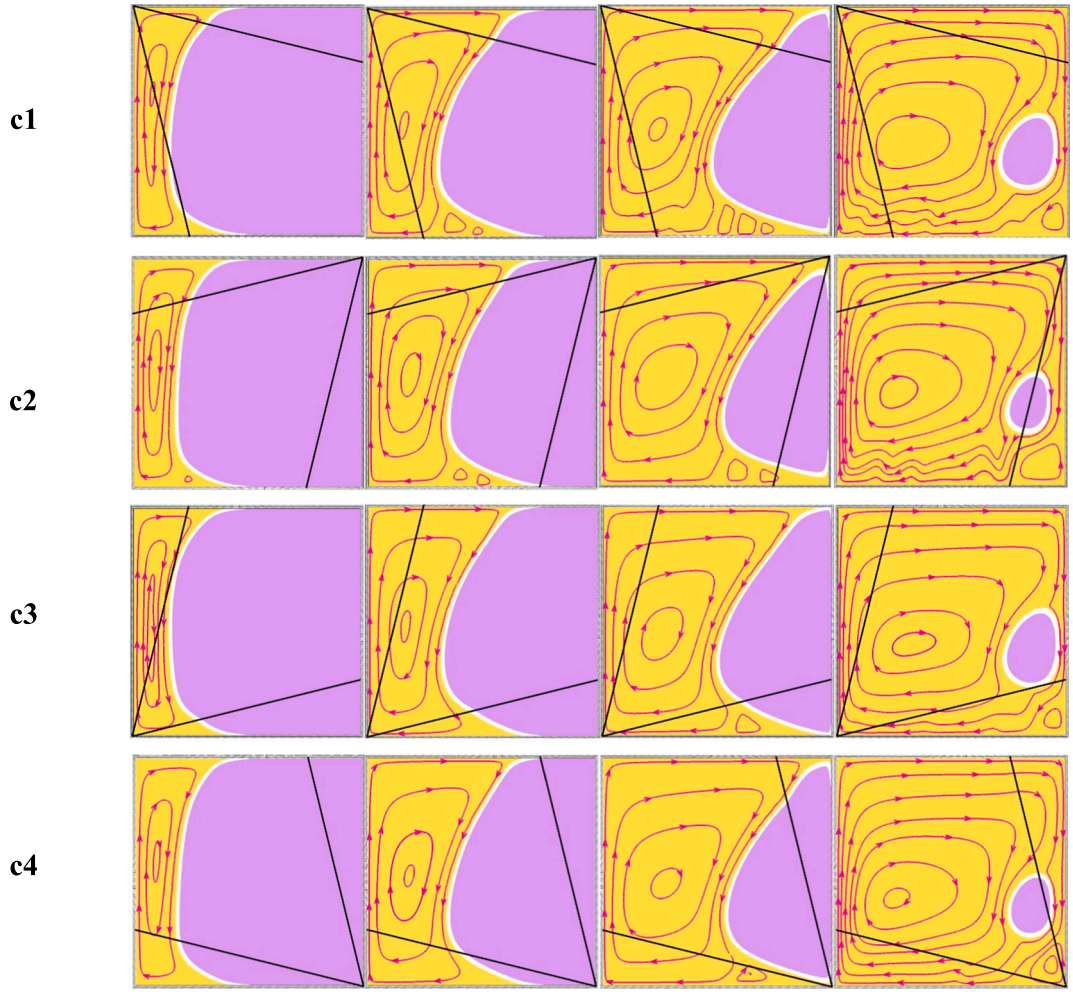

Fig. 11. (*continued*).

CRediT authorship contribution statement

Hakim S. Sultan Aljibori: Writing – review & editing, Visualization, Methodology, Investigation, Formal analysis, Conceptualization. **Ahmad Hajjar:** Writing – original draft, Methodology, Investigation, Formal analysis, Conceptualization. **Zehba Raizah:** Writing – original draft, Methodology, Investigation, Formal analysis, Conceptualization. **Faisal Alresheedi:** Writing – review & editing, Writing – original draft, Investigation, Formal analysis, Data curation, Conceptualization. **Ali Akremi:** Visualization, Validation, Resources, Methodology, Investigation, Formal analysis, Conceptualization. **Ahmed Elhassanein:** Writing – review & editing, Resources, Methodology, Investigation, Funding acquisition, Formal analysis. **Mohammad Ghalambaz:** Writing – review & editing, Writing – original draft, Supervision, Project administration, Conceptualization.

Declaration of competing interest

The authors clarify that there is no conflict of interest for report.

Acknowledgements

The authors extend their appreciation to the Deanship of Research and Graduate Studies at King Khalid University for funding this work through large Research Group Project under the grant number (RGP2/198/45). The authors extend their appreciation to the Deanship of Scientific Research at Northern Border University, Arar, KSA for funding this research work through the project number NBU-FFR-2025-2246-01. The authors are thankful to the Deanship of Graduate Studies and Scientific Research at University of Bisha for supporting this work through the Fast-Track Research Support Program.

Data availability

No data was used for the research described in the article.

References

[1] X. Hu, X. Gong, F. Zhu, X. Xing, Z. Li, X. Zhang, Thermal analysis and optimization of metal foam PCM-based heat sink for thermal management of electronic devices, Renew. Energy 212 (2023) 227–237.
[2] C. Zhao, J. Wang, Y. Sun, S. He, K. Hooman, Fin design optimization to enhance PCM melting rate inside a rectangular enclosure, Appl. Energy 321 (2022) 119368.
[3] H.A. Al-Salami, N.S. Dhaidan, H.H. Abbas, F.N. Al-Mousawi, R.Z. Homod, Review of PCM charging in latent heat thermal energy storage systems with fins, Ther. Sci. Eng. Prog. (2024) 102640.
[4] C. Zhao, M. Opolot, M. Liu, J. Wang, F. Bruno, S. Mancin, K. Hooman, Review of analytical studies of melting rate enhancement with fin and/or foam inserts, Appl. Therm. Eng. 207 (2022) 118154.
[5] M. Opolot, C. Zhao, P.F. Keane, M. Liu, S. Mancin, F. Bruno, K. Hooman, Discharge performance of a high temperature phase change material with low-cost wire mesh, Appl. Therm. Eng. 223 (2023) 120050.
[6] K. Liu, C. Wu, H. Gan, C. Liu, J. Zhao, Latent heat thermal energy storage: theory and practice in performance enhancement based on heat pipes, J. Energy Storage 97 (2024) 112844.
[7] A. Aziz, W. Waheed, A. Mourad, A. Aissa, O. Younis, E. Abu-Nada, A. Alazzam, Contemporary nano enhanced phase change materials: classification and applications in thermal energy management systems, J. Energy Storage 75 (2024) 109579.

[8] P. Du, M. Wang, X. Zhong, B. Chen, Z. Li, R. Zhou, Y. Huo, Z. Rao, Anisotropic porous skeleton for efficient thermal energy storage and enhanced heat transfer: experiments and numerical models, J. Energy Storage 56 (2022) 106021.
[9] W. Li, Y. Li, T. Yang, T. Zhang, F. Qin, Experimental investigation on passive cooling, thermal storage and thermoelectric harvest with heat pipe-assisted PCM-embedded metal foam, Int. J. Heat Mass Transf. 201 (2023) 123651.
[10] B. Öztürk, Z. Gölbaşı, M.Y. Yazıcı, Experimental investigation of the melting performance of a low porosity metal foam/PCM composite heat sink in various configurations, Int. Commun. Heat Mass Transf. 149 (2023) 107169.
[11] S. Sabet, B. Buonomo, M.A. Sheremet, O. Manca, Numerical investigation of melting process for phase change material (PCM) embedded in metal foam structures with Kelvin cells at pore scale level, Int. J. Heat Mass Transf. 214 (2023) 124440.
[12] A. NematpourKeshteli, M. Iasiello, G. Langella, N. Bianco, Using metal foam and nanoparticle additives with different fin shapes for PCM-based thermal storage in flat plate solar collectors, Ther. Sci. Eng. Prog. (2024) 102690.
[13] G. Shu, T. Xiao, J. Guo, P. Wei, X. Yang, Y.-L. He, Effect of charging/discharging temperatures upon melting and solidification of PCM-metal foam composite in a heat storage tube, Int. J. Heat Mass Transf. 201 (2023) 123555.
[14] G. Liu, T. Xiao, P. Wei, X. Meng, X. Yang, J. Yan, Y.-L. He, Experimental and numerical studies on melting/solidification of PCM in a horizontal tank filled with graded metal foam, Sol. Energy Mater. Sol. Cells 250 (2023) 112092.
[15] Y. Shuai, C. Zhang, X. Hu, S. He, X.-L. Gong, A comprehensive structural parameter for optimization of thermal performance of PCM embedded in periodic cuboid cell metal foam, Int. Commun. Heat Mass Transf. 146 (2023) 106936.
[16] Z. Bian, F. Hou, J. Chen, H. Wang, Numerical analysis on the effect of graded porosity in closed-cell metal foams/PCM composites, Case Stud. Ther. Eng. 55 (2024) 104145.
[17] C. Zhao, M. Opolot, M. Liu, F. Bruno, S. Mancin, K. Hooman, Phase change behaviour study of PCM tanks partially filled with graphite foam, Appl. Therm. Eng. 196 (2021) 117313.
[18] B. Kurşun, M. Balta, K. Karabulut, Exploring the impact of inner and middle channel geometries on the melting rate of PCM-metal foam composition in a triplex tube heat exchanger, Ther. Sci. Eng. Prog. 51 (2024) 102621.
[19] C. Zhao, M. Opolot, M. Liu, J. Wang, F. Bruno, S. Mancin, K. Hooman, Periodic structures for melting enhancement: observation of critical cell size and localized melting, Int. J. Heat Mass Transf. 195 (2022) 123107.
[20] T. Xiao, Z. Du, L. Lu, Y. Li, X. Huang, X. Yang, Y.-L. He, Melting of phase change materials inside metal foams with uniform/graded porosity: pore-scale simulation, Appl. Therm. Eng. 232 (2023) 121082.
[21] Z. Haddad, F. Iachachene, M.A. Sheremet, E. Abu-Nada, Numerical investigation and optimization of melting performance for thermal energy storage system partially filled with metal foam layer: new design configurations, Appl. Therm. Eng. 223 (2023) 119809.
[22] C. Yang, Y. Xu, X.-R. Xu, M. Bake, C.-M. Wu, Y.-R. Li, J.-J. Yu, Melting performance analysis of finned metal foam thermal energy storage tube under steady rotation, Int. J. Heat Mass Transf. 226 (2024) 125458.
[23] N.S. Bondareva, M.A. Sheremet, Numerical simulation of heat transfer performance in an enclosure filled with a metal foam and nano-enhanced phase change material, Energy 296 (2024) 131123.
[24] M. Ghalambaz, M. Sheremet, K. Shank, S. Tiari, M. Fteiti, Improving phase change heat transfer in an enclosure partially filled by uniform and anisotropic metal foam layers, Int. J. Heat Mass Transf. 228 (2024) 125678.
[25] M. Bouzidi, M. Sheremet, K. Shank, S. Tiari, M. Ghalambaz, Charging and discharging heat transfer improvement of shell-tube storage utilizing a partial layer of anisotropic metal foam, J. Energy Storage 79 (2024) 109948.
[26] S. Zhang, Y. Yao, Y. Jin, Z. Shang, Y. Yan, Heat transfer characteristics of ceramic foam/molten salt composite phase change material (CPCM) for medium-temperature thermal energy storage, Int. J. Heat Mass Transf. 196 (2022) 123262.
[27] M. Ghalambaz, A.A. Melaibari, A.J. Chamkha, O. Younis, M. Sheremet, Phase change heat transfer and energy storage in a wavy-tube thermal storage unit filled with a nano-enhanced phase change material and metal foams, J. Energy Storage 54 (2022) 105277.
[28] D.A. Nield, A. Bejan, Convection in Porous Media, Springer, 2006.
[29] C. Zhao, Y. Sun, J. Wang, K. Hooman, The applicability of volume-averaging method to simulate melting in a multi-scaled periodic structure, Energy 248 (2022) 123636.
[30] Y. Yao, H. Wu, Interfacial heat transfer in metal foam porous media (MFPM) under steady thermal conduction condition and extension of Lemlich foam conductivity theory, Int. J. Heat Mass Transf. 169 (2021) 120974.
[31] M. Ghalambaz, M. Aljaghtham, A.J. Chamkha, A. Abdullah, A. Alshehri, M. Ghalambaz, An anisotropic metal foam design for improved latent heat thermal energy storage in a tilted enclosure, Int. J. Mech. Sci. 107830 (2022).
[32] A.I.N. Korti, H. Guellil, Experimental study of the effect of inclination angle on the paraffin melting process in a square cavity, J. Energy Storage 32 (2020) 101726.
[33] A. Agarwal, R. Sarviya, Characterization of commercial grade paraffin wax as latent heat storage material for solar dryers, Mater. Today Proc. 4 (2) (2017) 779–789.
[34] N. Ukrainczyk, S. Kurajica, J. Šipušić, Thermophysical comparison of five commercial paraffin waxes as latent heat storage materials, Chem. Biochem. Eng. Q. 24 (2) (2010) 129–137.
[35] Y. Yao, H. Wu, Macroscale modeling of solid–liquid phase change in metal foam/paraffin composite: effects of paraffin density treatment, thermal dispersion, and interstitial heat transfer, J. Ther. Sci. Eng. Appl. 13 (4) (2021).
[36] N.B. Khedher, M. Sheremet, A.M. Hussin, S.A.M. Mehryan, M. Ghalambaz, The effect of hot wall configuration on melting flow of nano-enhanced phase change material inside a tilted square capsule, J. Energy Storage 69 (2023) 107921.
[37] H. Zheng, C. Wang, Q. Liu, Z. Tian, X. Fan, Thermal performance of copper foam/paraffin composite phase change material, Energy Convers. Manag. 157 (2018) 372–381.